

# Growth of CdZnTe single crystals by seed travelling heater method

XIAO GAO<sup>a</sup>, DONGXIAO TENG<sup>a</sup>, JUNCHENG LIU<sup>a, b\*</sup>, SHENQIU ZHAI<sup>c</sup>

<sup>a</sup>*School of Materials Science and Engineering, Shandong University of Technology, Zibo 255049, China*

<sup>b</sup>*School of Materials Science and Engineering, Tianjin Polytechnic University, Tianjin 300387, China*

<sup>c</sup>*School of Mechanical Engineering, Shandong University of Technology, Zibo 255049, China*

Cadmium zinc telluride crystal has attracted more and more attention due to its wide application in the areas of nuclear radiation detection, infrared detection, and high energy physics and so on. And it has been used for the epitaxial substrate of HgCdTe detectors with high performance whereby the molar ratio of Cd:Zn:Te is 0.96:0.04:1, particularly. At present, CdZnTe crystals are usually grown by Bridgman method, which often causes some problems, such as large Cd vacancy defects and high dislocation density. CdZnTe crystals with the dimensions of  $\Phi 39$  mm $\times$ 65 mm were grown by travelling heater method with seed crystal. The morphology of Te inclusions, as well as the dislocation density of the crystal was investigated. The infrared transmittance of the crystal was measured. The dislocation density was  $6.49 \times 10^5$  cm<sup>-2</sup>. Pentagonal Te inclusions or hexagonal Te inclusions were the main defects in the CdZnTe crystals. The average infrared transmittance of wafer was about 45%. In general, the crystal ingot quality was rather satisfying.

(Received November 28, 2017; accepted June 14, 2019)

*Keywords:* Cadmium zinc telluride crystal, Seed travelling heater method, Seed crystal, Infrared transmittance, Dislocation density

## 1. Introduction

As an important semiconductor material, CdZnTe has received increasing attention due to its broad application in the field of nuclear radiation detection, infrared detection, high-energy physics, etc [1]. For instance, Cd<sub>0.9</sub>Zn<sub>0.1</sub>Te single crystals have been employed to fabricate room temperature X-ray detectors and  $\gamma$ -ray detectors [2]. Cd<sub>0.96</sub>Zn<sub>0.04</sub>Te single crystals are commonly used as substrate material for preparation of high performance infrared HgCdTe detectors [3]. Thanks to its excellent optoelectronic properties, CZT single crystal has become an ideal material for semiconductor photodetectors with suitable bandwidth.

However, CZT-based detectors often require high-quality single crystals with homogeneous composition and large size. In addition, the manufacturing cost needs to be reasonably low. In order to obtain large size CZT crystals, the growth techniques have been extensively studied by researchers. Sun et al. [4] prepared Cd<sub>0.2</sub>Zn<sub>0.8</sub>Te crystals by the temperature gradient solution growth (TGSG) method. The growth interface of the crystal was smooth, and the density of Te inclusion within the ingot was significantly reduced. Moreover, the resistivity and infrared transmittance of the crystals were maintained at a high level by optimizing the crucible descending rate. Shkir et al. [5] prepared CZT crystals by the vertical gradient freeze (VGF) method, and studied the crystallinity and

mechanical properties of the CZT crystals. It was found that the mechanical properties of CZT were better than some device-level materials. Other researchers used high-pressure Bridgman method [6, 7] and low-pressure Bridgman method [8] to prepare CZT crystals. It was found that the crystals prepared by these methods had higher carrier mobility and excellent optoelectronic performance. However, there are some challenges remaining in the crystal growth process such as high Cd vapor pressure, high temperature, poor heat transfer, Zn segregation, etc. These issues significantly affect the crystal quality and yield. In addition, the production cost is often high. Thus, with the conventional melt method, it is still difficult to prepare CZT crystal with large size, high quality, and homogeneous composition for commercial application.

Recently, the traveling heater method (THM) has been proposed as a promising method to prepare high quality CZT crystals [9]. THM combines the advantages of both liquid phase epitaxy and zone purification, and improves the crystal's composition homogeneity as well [10, 11]. As Te is used as the solvent, the crystal growth temperature of THM is much lower than the melting point of the crystal. Therefore, the vapor pressure in the crucible decreases, and the impurity diffusing from the inner wall of crucible is partly excluded. Both the crucible bursting danger and the dislocation density of the crystal are also reduced. Instead of melting, the polycrystalline ingot in contact with the solvent zone

begins to melt (Fig. 1). The solute flows down through the solvent zone, and crystallizes at the growth interface. As the temperature field moves up, the solvent zone is also slowly moved up, and finally the crystal growth process is completed. However, the growth rate of THM must be very slow (about 1~5 mm / day) [12-14]. Schoenholz et al. [15] reported that the etch pit density of CdTe crystal prepared by THM was significantly lower than that prepared by Bridgman method. Lai et al. [16] prepared  $\text{Cd}_{0.9}\text{Mn}_{0.1}\text{Te}$  crystals with THM. It was found that THM could improve the distribution of Mn in the axial direction of the ingot, and the resistivity of the crystal was  $(1.5-8) \times 10^{10} \Omega \cdot \text{cm}$ . Chen et al. [17] tested CZT crystals using low-temperature photoluminescence spectrum, and found that crystal prepared by THM had lower defect density, and the defect was distributed uniformly. Roy et al. [18] prepared CdTeSe crystals by THM using Te as solvent. The results showed that there were fewer sub-grain interfaces in the crystal, and the crystal quality was not affected by the stress from the inner wall of the crucible. In addition, Te solvent zone could remove polycrystalline impurities, and played a role of regional purification [19]. So far, the solvent used to prepare CZT crystals by THM is pure Te solvent. However, the solubility of Cd and Zn in pure Te solvent is very high, and the seed crystals can also be dissolved by pure Te solvent. The adductive crystallization of seed crystal will be affected, and the crystal quality is reduced.

In this study, CZT crystals were prepared by seed THM (STHM) with modified Te solvent. The ingot structure evolution process, Te inclusion morphology, and dislocation density within the CZT crystal were investigated and analyzed. The infrared transmittance of the CZT crystals was measured. Furthermore, the optical performance of the crystals prepared by STHM was compared to that of the CZT crystals prepared with conventional vertical Bridgman methods.

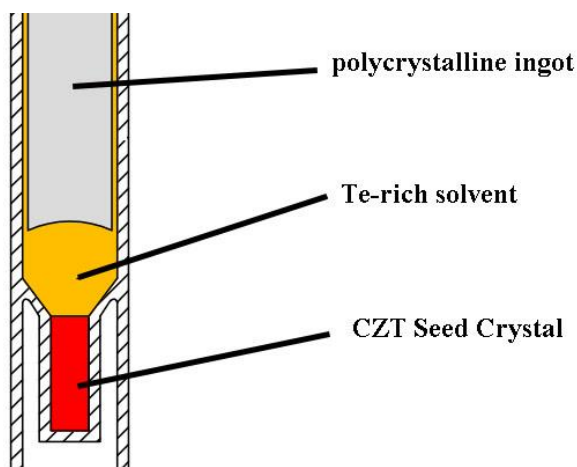


Fig. 1. The arrangement of seed and various components in the quartz crucible

## 2. Experimental methods

### 2.1. CZT ingot growth

First, the CZT seed crystal was fixed in the bottom of the quartz crucible. The CZT seed crystal was prepared by the vertical Bridgman method with crystal orientation of (110). The Te-rich solvent with Cd (the molar ratio of Cd to Te is 3:17) instead of pure Te solvent was placed above the seed crystal. The Te-rich solvent can reduce the dissolution rate of the seed crystal. In addition, it can also prevent the loss of the seed crystal. The polycrystalline ingot was placed above the Te-rich solvent. The evacuation and sealing operation of the quartz crucible were carried out. Subsequently, the quartz crucible was placed in the crystal growth furnace. The Te-rich solvent zone was located at the highest temperature zone of the furnace. The crystal growth rate was 5 mm/day, and the temperature gradient at the growth interface was about 6 °C/cm.

### 2.2. Crystal ingot slicing

The hardness of CZT is rather poor, so the crystal ingot is easy to break. A diamond-wire slicer is used to cut the ingot into wafers. The cutting direction was perpendicular to the growth axis of the crystal ingots. The thickness of each wafer was 2 mm. The wafers were labeled from the ingot bottom to the top as CZT-1, CZT-2, and CZT-3.

### 2.3. Characterization

The wafers were mechanically polished using a precision polisher to remove scratches on the wafer surface. Next, the wafers were chemically etched to remove the mechanical damage and oxide layers on the wafer surface. The Te inclusion on the wafer surface was observed by metallographic microscope. The infrared transmittance of the wafers was measured with a Thermo Electron Nicolet 7500 Fourier Infrared Transform Spectrometer. The wave number ranges from  $400 \text{ cm}^{-1}$  to  $4000 \text{ cm}^{-1}$ .

## 3. Results and discussion

### 3.1. Effect of Te-rich solvent on seed crystal

Fig. 1 shows the CZT ingot prepared by STHM, and the seed crystal before and after growth. It is clear that after growth, the residual seed was surrounded by a layer of Te solvent, so its diameter increased from 9.79 mm to 12.16 mm. Therefore, it is deduced that only a small portion of the seed crystal dissolved at the beginning of the growth process.



Fig. 2. CZT crystal ingot and seed crystal before and after growth. (a) CZT crystal ingot; (b) Seed crystal before growth; (c) Seed crystal after growth

### 3.2. Ingot structure evolution process



Fig. 3. Macro morphologies of the CZT wafers at different positions of the ingot

Fig. 3 shows the macro morphology of the CZT wafers at different positions of the ingot. As shown in Fig. 4, the silver-white region is Te solvent residue, which may melt after 5 hours at 700 °C, and the black region is CZT crystal. The Te solvent is around the CZT wafer, and its distribution range is relatively large. This is because that the moving rate of the temperature field was high, the nucleation process at the radial direction was not completed in time. The content of Te in the solute transferred from the dissolution interface to the growth

interface through the solvent zone was increased, and the CZT crystal was coated by the excess Te solvent. Hence, some Te solvent remains around the wafers. The morphology of the CZT wafers in Fig. 2 shows that the ratio of CZT crystal at the ingot top position reduces. This might be mainly because that the Cd concentration in the solvent decreases.

### 3.3. Te inclusion morphology within the CZT crystals

Fig. 4 shows the micro morphology of the CZT wafers. It can be seen that there are a lot of Te inclusions or Te deposits within the crystal ingot. This might be attributed to the low temperature gradient in front of the growth interface, which resulted in a low solute concentration gradient. Therefore, Te solvent zone could not be moved with the moving of the temperature field, and the Te solvent was intercepted among the CZT crystal to form inclusions. As shown in Fig. 4, there are several types of Te inclusions or Te deposits existing in the wafer (the white region in the figure). It is also found that the pentagonal Te inclusions or hexagonal Te inclusions were the main defects in the CZT crystals.

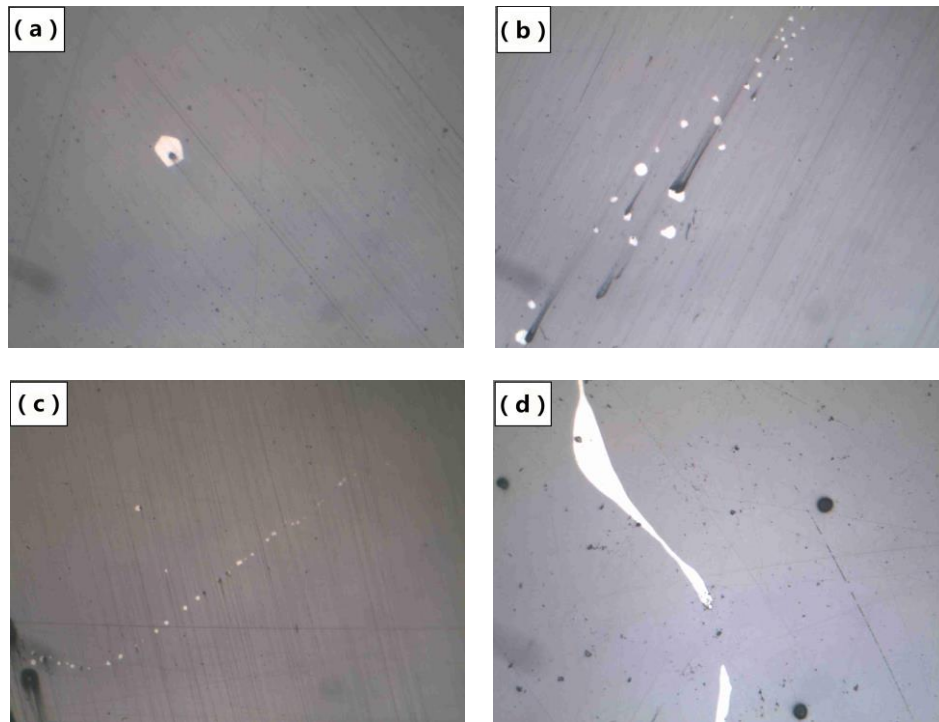


Fig. 4. Microstructure of CZT wafers ( $\times 200$ ): (a) Pentagon Te inclusion; (b) Flake Te inclusion; (c) Linear Te inclusion (d) Strip Te inclusion

### 3.4. Analysis of dislocation density in CZT wafers

The dislocation density is the total length of dislocation lines in a unit volume of crystals. That is, as in Equation (1):

$$D_d = \frac{L}{V} \quad (1)$$

where  $D_d$  is the dislocation density ( $\text{cm}^{-2}$ ),  $L$  is the total length of the dislocation line in the crystal, and  $V$  is the volume of the crystal. The etch pits are the outcrops of the dislocations on the wafer surface, and there is a one-to-one correlation between etch pit and dislocation. The dislocation density is usually expressed by etch pit density (EPD). That is, as in Equation (2):

$$D_d = EPD = \frac{N \times M_i}{S} \quad (2)$$

where  $N$  is the magnification of the microscope,  $S$  is the measured field area, and  $M_i$  is the number of etching pits in the field of view. The EPD is calculated by Equation (2), and the results are shown in Table 1. Where  $D_{d1}$  is the dislocation density of the CZT prepared by STHM, and  $D_{d2}$  is the dislocation density of the CZT growth from solution [20].

It can be seen from Fig. 5 that the dislocation density of the ingot prepared by STHM is relatively homogeneous, and there are little changes of dislocation density at different position. The impurity can be purified by Te-rich solvent in the crystal growth process, and the

solute can also be buffered by Te-rich solvent. The growth condition of the crystal is relatively steady. However, Table 1 shows that the  $D_{d1}$  is in the range of  $10^5$  to  $10^6 \text{ cm}^{-2}$ . Compared to  $D_{d2}$ , the dislocation density of the ingot prepared by STHM is larger than that of the ingot grown from solution. The main reasons for the formation of dislocations in crystals are as follows [21]: (1) thermal stress caused by temperature gradients during growth; (2) thermal expansion coefficient mismatch between crystals and crucibles; (3) lattice mismatch caused by composition inhomogeneous within the crystal. Fig. 3 shows that the number of Te inclusions at the top position of the ingot is large. The lattice distribution of CZT crystal is affected by these Te inclusions, and the dislocation density is increased. Besides, the crystal contacts with the inner wall of the crucible directly in the growth process. The thermal expansion coefficient of crystal and crucible does not match, causing the increase of the dislocation density in the crystals.

### 3.5. Analysis of infrared transmittance

The infrared transmittance is affected by diffuse reflection which is caused by rough surface. Before to be measured, the CZT wafers were polished and cleaned in order to attain a mirror surface.

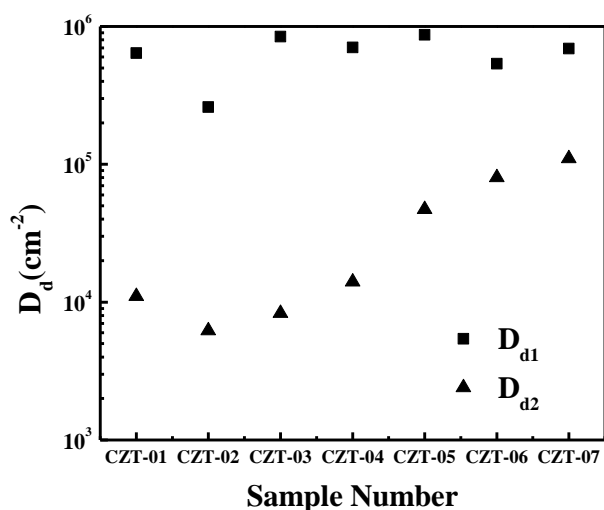


Fig. 5. Distribution map of dislocation of wafers

Table.1. The dislocation density of wafers

Sample number	CZT-01	CZT-02	CZT-03	CZT-04	CZT-05	CZT-06	CZT-07
$D_{d1}$ ( $\text{cm}^{-2}$ )	$6.4 \times 10^5$	$2.6 \times 10^5$	$8.45 \times 10^5$	$7.04 \times 10^5$	$8.70 \times 10^5$	$5.37 \times 10^5$	$6.91 \times 10^5$
$D_{d2}$ ( $\text{cm}^{-2}$ )	$1.1 \times 10^4$	$6.2 \times 10^3$	$8.3 \times 10^3$	$1.4 \times 10^4$	$4.7 \times 10^4$	$8.0 \times 10^4$	$1.1 \times 10^5$

There are two main infrared absorption mechanisms for an intrinsic CZT wafer: the lattice absorption and the free carrier absorption. The lattice absorption plays a major role near the wave number  $4000 \text{ cm}^{-1}$ . As shown in Fig. 6, the infrared transmittance of sample 2 is larger than that of sample 1. The variation trend of the two samples is very similar, and the infrared transmittance increases with the increase of wavenumber. However, the average infrared transmittance of these two samples is small, and the effect of Te inclusions on it is large. The lattice arrangement within crystal can be changed by Te inclusion, and the lattice consistency will be disrupted. As a result, there are a number of dislocations forming within the crystal. The infrared light will be absorbed because the number of dislocation is large and the scattering phenomenon dominates. Hence, the infrared transmittance is relatively low. Reference [22] shows that the infrared transmittance pattern showing an up-spread type means the resistivity of wafer is low (about  $4.0 \times 10^7 \sim 5.7 \times 10^7 \Omega \cdot \text{cm}$ ). Xu et al. [23] prepared CZT crystal by modified seed-vertical Bridgman method, and the infrared transmittance of wafers was measured. It was found that the infrared transmittance of the samples did not increase with the increase of wavenumber and the average value was 62%. This means that the number of Te inclusions within the ingot was small, the dislocation density was low and the phenomenon of lattice mismatch was unusual. Besides, the resistivity of the wafer was high, and the comprehensive performance was decent.

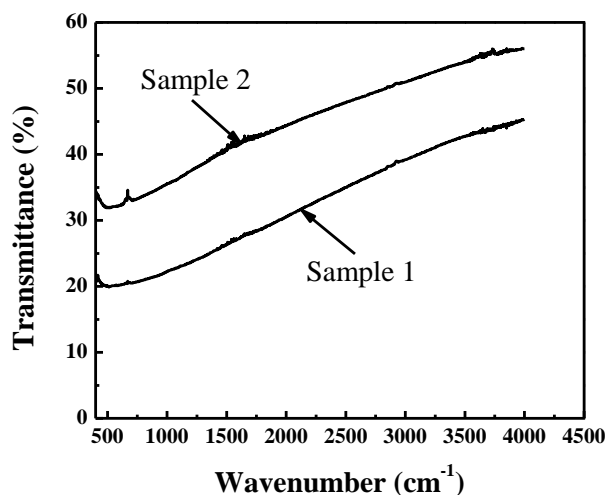


Fig. 6. Infrared transmittance spectra of different sample wafers

#### 4. Conclusions

CZT crystals ( $\Phi 39 \text{ mm} \times 65 \text{ mm}$ ) were successfully prepared by STHM with Te-rich solvent. The size of the seed crystals before and after the growth, the macro and micro morphology of the CZT wafers, and dislocation density were investigated. In addition, the infrared transmittance of the wafers was measured. The results are shown as follows:

(1) The size of seed crystal changed a little before and after the growth. The seed crystal was not completely dissolved, and the residual seed was surrounded by a layer of Te solvent.

(2) As shown in the macro morphology of the wafers, Te solvent was distributed around the CZT wafer, and its distribution range was relatively large. There was large amount of Te solvent at the top position of the ingot.

(3) Seen from the micro morphology of wafers, there were a large amount of Te inclusions within the crystal ingot. Pentagonal Te inclusions or hexagonal Te inclusions were the main defects in the CZT crystals.

(4) Dislocation density calculated by EPD equation of ingot was  $6.49 \times 10^5 \text{ cm}^{-2}$ , and the distribution of dislocation density within the ingot was relatively homogeneous. Nevertheless, the dislocation density of the CZT crystal ingot prepared by STHM was much higher than that of CZT crystal ingot grown from solution.

(5) The infrared transmittance spectrum shows that the infrared transmittance of CZT crystal prepared by seed crystal-THM is higher than that prepared by vertical Bridgman method, and the average infrared transmittance of the wafer is about 45%.

Overall, the growth rate of 5 mm/day was too fast for a temperature gradient of 6 °C/cm and a crystal interface temperature of 700 °C, so that the crystal could not fill the crucible, and Te solvent could not be discharged immediately. There were a large amount of Te inclusions within the ingot, and the dislocation density was large. The infrared transmittance of the wafers was also influenced.

### Acknowledgements

This work was supported by the National Natural Science Foundation of China (No.50972085), Key R & D project of Shandong Province (No. 2017GGX20104).

### References

- [1] S. D. Sordo, L. Abbene, E. Caroli, A. M. Mancini, A. Zappettini, P. Ubertini, *Sensors* **9**, 3491 (2009).
- [2] X. C. Zhao, X. P. Ouyang, Y. D. Xu, H. T. Han, Z. C. Zhang, T. Wang, G. Q. Zha, X. Ouyang, *AIP Adv.* **2**, 012162 (2012).
- [3] J. MacKenzie, F. J. Kumar, H. Chen, *J. Electron. Mater.* **42**, 3129 (2013).
- [4] X. X. Sun, J. H. Min, X. Y. Liang, T. Zhang, J. Q. Teng, J. J. Zhang, L. J. Wang, *Adv. Mater. Res.* **634-638**, 2470 (2013).
- [5] M. Shkir, V. Ganesh, S. AlFaify, A. Black, E. Dieguez, G. Bhagavannarayana, *J. Alloys Compd.* **686**, 438 (2016).
- [6] I. Nasieka, N. Kovalenko, V. Kutniy, A. Rybka, D. Nakonechnyj, S. Sulima, V. Strelchuk, *Sens. Actuators A* **203**, 176 (2013).
- [7] K. H. Kim, J. H. Choi, A. E. Bolotnikov, G. S. Camarda, A. Hossain, G. Yang, Y. Cui, R. B. James, *J. Korean Phys. Soc.* **62**, 623 (2013).
- [8] M. Jeong, H. S. Kim, Y. S. Kim, J. H. Ha, *J. Korean Phys. Soc.* **64**, 1105 (2014).
- [9] Z. Y. Li, J. H. Peterson, A. Yeckel, J. J. Derby, *J. Cryst. Growth* **452**, 17 (2016).
- [10] M. Amman, J. S. Lee, P. N. Luke, H. Chen, S. A. Awadalla, R. Redden, G. Bindley, *IEEE Trans. Nucl. Sci.* **56**, 795 (2009).
- [11] H. Shiraki, M. Funaki, Y. Ando, A. Tachibana, S. Kominami, R. Ohno, *IEEE Trans. Nucl. Sci.* **56**, 126 (2008).
- [12] W. Q. Wu, J. J. Zhang, L. J. Wang, J. H. Min, X. Y. Liang, X. L. Wen, *Phys. Status Solidi* **158**, 412 (2016).
- [13] A. Nagaoka, Y. Nose, H. Miyake, M. A. Scarpulla, K. Yoshino, *Renewable Energy* **79**, 127 (2014).
- [14] W. Liang, K. F. Qin, J. J. Zhang, H. Meng, W. Q. Wu, X. Y. Liang, J. H. Min, L. J. Wang, *J. Cryst. Growth* **419**, 123 (2015).
- [15] R. Schoenholz, R. Dian, R. Nitsche, *J. Cryst. Growth* **72**, 72 (1985).
- [16] J. M. Lai, J. J. Zhang, L. J. Wang, J. H. Min, W. Q. Wu, M. Shen, W. Liang, *Cryst. Res. Technol.* **50**, 817 (2015).
- [17] X. Chen, T. Wang, B. R. Zhou, J. He, Y. Li, F. Yang, Y. D. Xu, G. Q. Zha, W. Q. Jie, *J. Synth. Cryst.* **42**, 2215 (2013).
- [18] U. N. Roy, A. E. Bolotnikov, G. S. Camarda, Y. Cui, A. Hossain, K. Lee, G. Yang, R. B. James, *J. Cryst. Growth* **389**, 99 (2014).
- [19] G. Yang, A. E. Bolotnikov, Y. Cui, G. S. Camarda, A. Hossain, R. B. James, *J. Cryst. Growth* **311**, 99 (2008).
- [20] D. Wang, J. H. Min, X. Y. Liang, W. W. Liu, J. J. Zhang, L. J. Wang, *J. Shanghai Univ.* **19**, 67 (2013).
- [21] G. D. Zhang, S. Q. Zhai, H. W. Cui, J. C. Liu, *J. Synth. Cryst.* **36**, 301 (2007).
- [22] G. Q. Li, W. Q. Jie, H. Hua, *J. Infrared Millimeter Waves* **22**, 469 (2003).
- [23] Y. D. Xu, W. Q. Jie, P. Sellin, T. Wang, L. Fu, G. Q. Zha, P. Veeramani, *IEEE Trans. Nucl. Sci.* **56**, 2808 (2009).

\*Corresponding author: jchliu@sdut.edu.cn